Contrasting Silicic Magma Series in Miocene-Pliocene Ash Deposits in the San Miguel de Allende Graben, Guanajuato, Mexico

Aaron J. Adams, Eric H. Christiansen,[1,2] *Bart J. Kowallis,*[2] *Oscar Carranza-Castañeda,*[3] *and Wade E. Miller*[2]

Anadarko Petroleum Corporation, P.O. Box 1330, Houston, Texas 77251-1330, U.S.A.
(e-mail: aaron.adams@anadarko.com)

ABSTRACT

The San Miguel de Allende graben, Guanajuato, Mexico, contains numerous rhyolitic volcanic ash beds. Electron microprobe and x-ray fluorescence analyses of glass shards from 14 localities, combined with mineralogic, stratigraphic, radiometric, and paleomagnetic data, allow us to correlate the ash beds (and the intervening sedimentary strata and fossils), understand the timing of volcanism, date the age of extension, and better understand the tectonic and volcanic evolution of central Mexico. Our analyses reveal that at least six separate eruptions of rhyolitic ash occurred during the Late Miocene and Pliocene (5–3 Ma) while the San Miguel Allende basin was subsiding. The fallout ash beds can be distinguished by phenocryst mineralogy, inferred eruption temperatures, and differences in major and trace element compositions. Two magma series (medium K and high K) are represented in the rhyolitic tephra deposits. The high-K series is marginally peralkaline, reduced (indicated by high Fe/Mg ratios), dry (paucity of hydrous silicates), hot (≤860°C), and enriched in many incompatible trace elements including Nb, Y, and Zr. They have the characteristics of anorogenic rhyolites formed in rift and hotspot settings. In contrast, the rhyolites of the medium-K series are similar to those erupted in subduction-related volcanic arcs. They are calcic to calc-alkalic with low Fe/Mg ratios and have hydrous phenocrysts, suggesting the water fugacity was also high. Eruption temperatures were less than ~860°C. However, these medium-K rhyolites have high Sr/Y ratios and were probably derived by differentiation of adakitic parents. We suggest the contrasting rhyolite series are the result of differentiation of two different parental magma types. During the late Miocene to Pliocene slab breakoff, hot asthenosphere rose through a break in a subducting slab of oceanic lithosphere. Parents of the medium-K series (adakitic magmas) formed as hot rising mantle caused the edge of the torn plate to melt. High-K parental magmas were formed by decompression melting as asthenospheric mantle rose through the gap in the slab.

Introduction

Volcanic ash beds can be important in several ways: they can provide regional markers for correlation, they can reveal the compositional and temporal evolution of crustal magma systems, and their mineral and glass compositions may reveal the tectonic setting in which their parental magmas formed. In this work, we focus on the compositions and phenocryst minerals of Neogene ash deposits in central Mexico as a prelude to using them as stratigraphic markers in a region rich in vertebrate fossil localities. The ash beds are petrologically significant in their own right, and these petrological aspects are the focus of the work reported here.

The presence of mafic magmatic rocks with intraplate affinities is a common feature of subduction-related orogenic belts. A brief episode of slab rollback or detachment provides an attractive explanation for their occurrence and contemporaneity with arclike magmas. Recently, Ferrari (2004) proposed that detachment and breakup of a subducting slab (the Rivera plate) beneath Mexico produced a pulse of Miocene (11–6 Ma) mafic volcanism that swept eastward across central Mexico. This was followed by trenchward migration of the volcanic front. A small fraction of the mafic volcanism related to this trenchward migration has an

Manuscript received May 17, 2004; accepted September 1, 2005.

[1] Author for correspondence; e-mail: eric_christiansen@byu.edu.

[2] Department of Geological Sciences, Brigham Young University, Provo, Utah 84602, U.S.A.

[3] Instituto de Geología, Universidad Nacional Autónoma de México, México 20, D.F. 04510, México.

[The Journal of Geology, 2006, volume 114, p. 247–266] 0022-1376/2006/11402-0007$15.00

intraplate alkaline affinity. However, the dominant volume of magma has a clear arclike continental margin signature. Ferrari et al. (2001) and Petrone et al. (2003) invoked partial melting of upwelling asthenosphere in the formation of the alkaline mafic magmas.

We pursue this notion further and examine the silicic fallout tuffs of late Miocene to Pliocene age that partially fill the San Miguel Allende graben, a small N-S-trending, fault-bounded basin north of the Trans-Mexican Volcanic Belt near Queretaro. We conclude that the silicic volcanic record complements the mafic component in that there are two distinctive types of contemporaneous silicic volcanism, one that is alkalic and intraplate in character and one that is a more typical convergent margin suite of calc-alkaline rhyolites. Their origin is consistent with the slab detachment hypothesis. Brief episodes of slab rollback and eventual detachment may be important in creating intraplate magmas in many collisional orogens, and these episodes may be recorded in fallout ash deposits.

Regional Geology

The Mexican state of Guanajuato and the San Miguel de Allende graben are in the southern Basin and Range extensional province (Kowallis et al. 1998) and near the northern margin of the present-day Trans-Mexican Volcanic Belt (fig. 1). During the early to middle Cenozoic, western North America was dominated by a subduction system along the western margin of the continent (Lipman et al. 1972; Snyder et al. 1976; Ferrari et al. 1994). Major eruptions of silicic ignimbrites occurred in the Great Basin region of Nevada and Utah, as well as Colorado, southwestern New Mexico, southern Arizona, and across most of western Mexico to create the Sierra Madre Occidental (Stewart 1978; Ferrari et al. 2001). About 20 Ma, the tectonic and igneous character of western North America changed markedly (Christiansen and Lipman 1972; Noble 1972; Allan 1986; Moore et al. 1994; Righter and Rosas-Elguera 2001). Basalt, or bimodal basalt and rhyolite assemblages, became dominant, and the initiation of extensional tectonics led to the development of the Gulf of Mexico and basin and range structures along the Western Cordillera of North America (Stewart 1978; Henry and Aranda-Gómez 1992).

The Trans-Mexican Volcanic Belt is a Neogene-Quaternary volcanic arc ~1000 km wide, stretching obliquely from east to west across Mexico at ~20°N latitude (Aguirre-Díaz et al. 1998; Pasquaré et al. 1991). It cuts across the southern margin of the middle Cenozoic volcanic rocks of the Sierra Madre Occidental (fig. 1), and it represents the reestablishment of a volcanic arc in southwestern Mexico related to subduction of the Cocos Plate along the Pacific margin of North America (Pasquaré et al. 1991; Ferrari et al. 1994). Abundant Quaternary composite volcanoes mark the arc. In central Mexico, the transition between volcanism related to the Sierra Madre Occidental and the Trans-Mexican Volcanic Belt occurred ~14 Ma (Cerca Martinez et al. 2000)

Most of the northern and middle portions of Mexico underwent extension in the late Cenozoic and are thus a significant portion of the Basin and Range Province of North America (Stewart 1978; Henry et al. 1991; Henry and Aranda-Gómez 1992). In Mexico, basin and range structures extend southward along either side of the Sierra Madre Occidental, leaving a high plateau (1,800–3,000 m) of relatively undeformed Cenozoic volcanic rocks (Stewart 1978). Mooser (1972) suggests that Basin and Range–like grabens have been developing in the northwest section of the Trans-Mexican Volcanic Belt since mid-Tertiary time, as evidenced by the cross-cutting relationships of fracture zones and faults. Ferrari et al. (2002) show that, at least in western Mexico, extension may have started ~21 Ma, but initiation could be as young as ~12 Ma. Mapping in the San Miguel de Allende region by Pasquaré et al. (1991), Carranza-Castañeda et al. (1994), and Cerca-Martínez et al. (1992) shows a predominant pattern of north-striking normal faults. Their orientation reinforces the suggestion of a southern continuation of the Basin and Range Province across this region (Henry and Aranda-Gómez 1992).

Local Geology

The city of San Miguel de Allende lies in the southeastern portion of a north-trending graben that is ~15 km wide and 20 km long. The basin lies in the southern Sierra Madre Occidental ~100 km north of the presently active part of the Trans-Mexico Volcanic Belt. It is bounded on both the eastern and western margins by fault-produced ridges that trend north (fig. 2). Displacement along the eastern fault zone exceeds 200 m in some areas of the basin and generally decreases to the south (Carranza-Castañeda et al. 1994). Roadcuts through Plio-Pleistocene sediments reveal smaller faults with individual offsets of 0.5–2.0 m and suggest continued extension in the region up to (or near to) the present time (Carranza-Castañeda et al. 1994). Zuniga et al. (2003) also concluded that

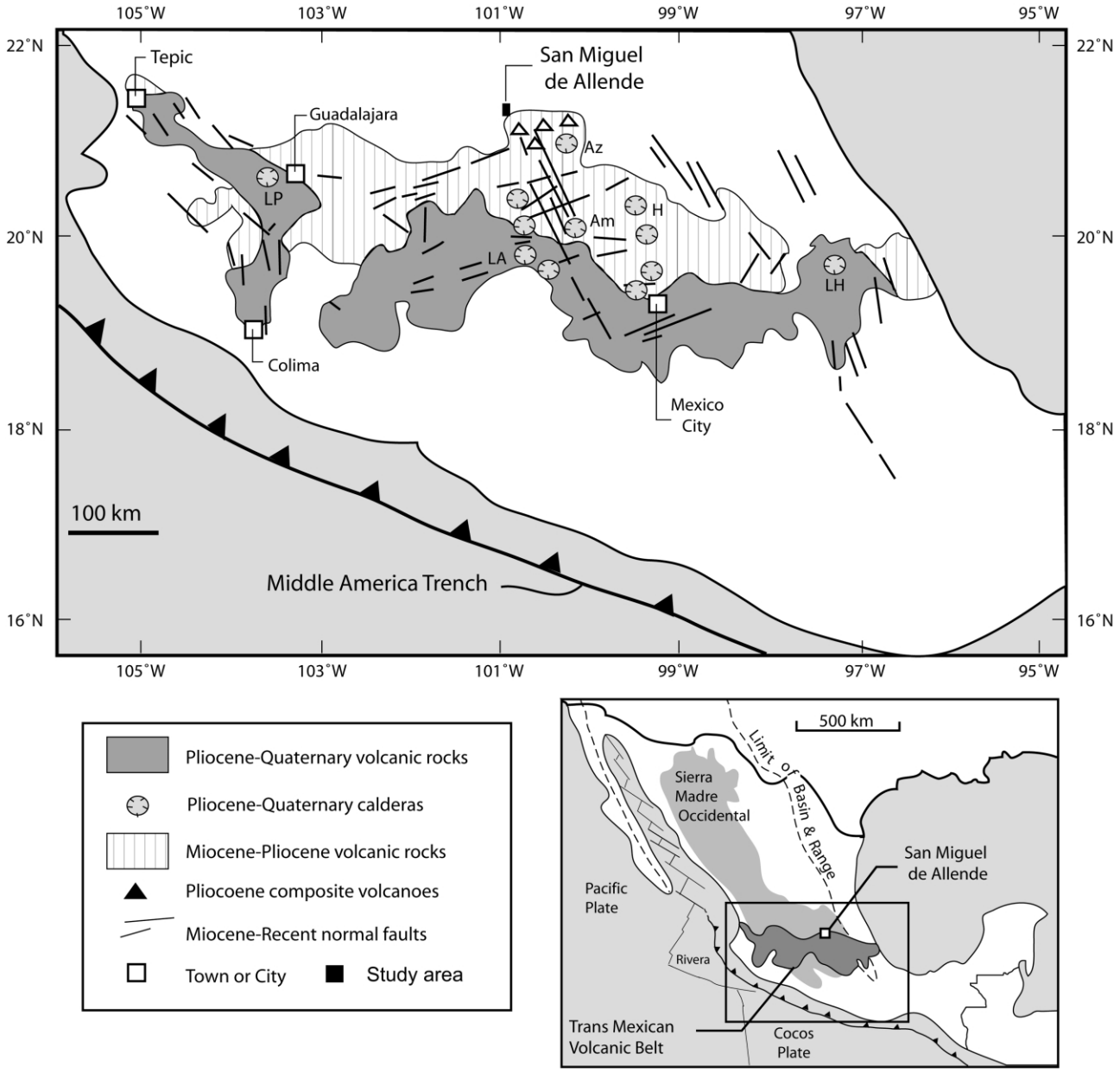

Figure 1. Map of central Mexico showing major calderas, volcanos, and fault systems along the Trans-Mexican Volcanic Belt. The San Miguel de Allende basin is located at the northern margin of the belt. Silicic calderas: *LP* = La Primavera, *LA* = Los Azufres, *Am* = Amealco, *Az* = Amazcala, *H* = Huichapan, *LH* = Los Humeros. Modified after Aguirre-Díaz and McDowell (2000) and Aguirre-Díaz and López-Martínez (2001).

the region contains seismically active faults. The fault zone forms part of the 250-km-long San Miguel de Allende–Catorce fault system, which, according to Nieto-Samaniego et al. (1999), separates the strongly deformed Mesa Central from the less extended Sierra Madre Oriental.

Carranza-Castañeda et al. (1994) indicate that the Tertiary volcanic rocks capping these fault-bounded ridges range in age between ~30 and 10 Ma. At the base is the 29-Ma Obraje ignimbrite of the Sierra Madre Occidental (Aranda-Gómez et al. 2003*a*). Perez-Vanzor et al. (1996) and Valdéz-Moreno et al. (1998) showed that the mountains to the south are underlain by 8–12-Ma andesitic to dacitic stratovolcanoes. These are among the oldest volcanoes in the Trans-Mexican Volcanic Belt and may be of ada-

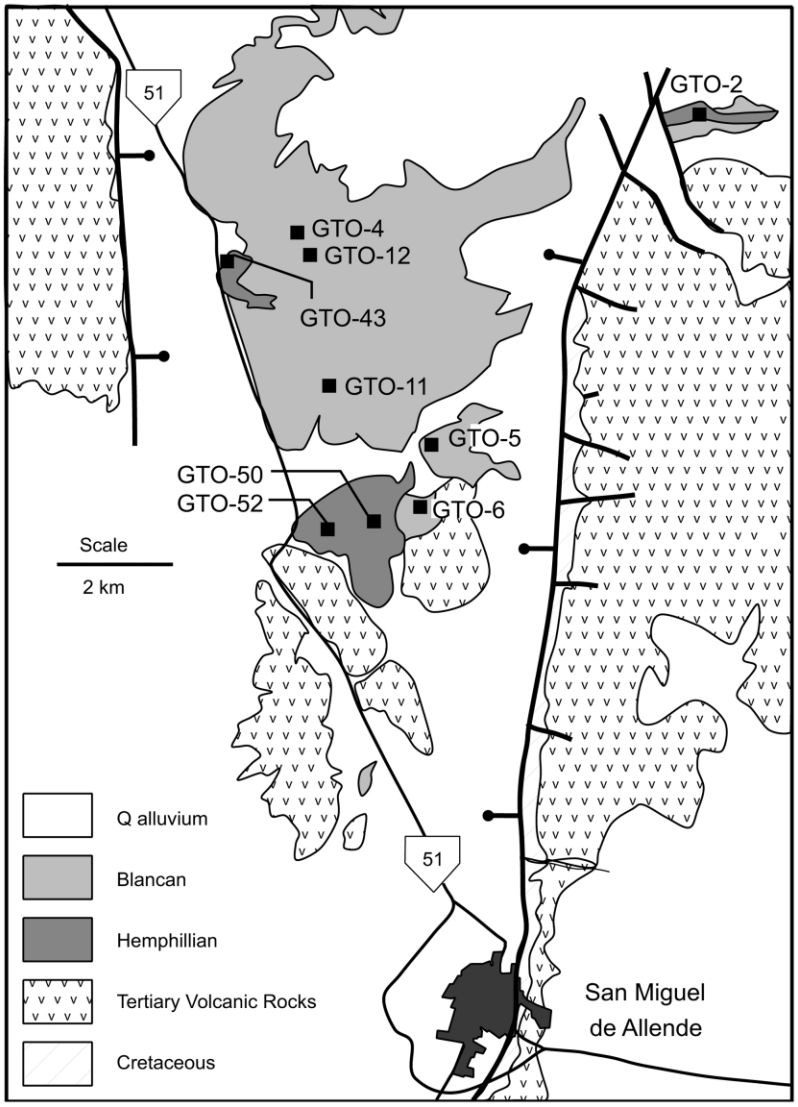

Figure 2. Generalized geologic map of the San Miguel Allende graben showing sample sites. Blancan and Hemphillian deposits include layers of fallout ash. Modified from Carranza-Castañeda et al. (1994).

kitic affinity (Gómez-Tuena et al. 2003; Ferrari 2004). They are partially buried by 6.2-Ma mafic lavas. Using fission track methods, Kowallis et al. (1986, 1998) analyzed the detrital zircon grain ages from three sediment/reworked ash samples within the basin and showed on an age probability plot that most of the grains fell into three groups. The first group of grains had a broad peak centered at ~25–30 Ma, the second group was at ~10–12 Ma, and the third was at 3–5 Ma. These ages reflect the local input of sediment into the basin from the older Tertiary volcanic rocks as well as the input of younger material from ash eruptions between 3 and 5 Ma. It is these younger ash beds that are the focus of this article.

The ash beds and fossils provide good age control and represent the most complete stratigraphic record of the Hemphillian (latest Miocene to earliest Pliocene) and Blancan (Pliocene) times found anywhere in North America (Kowallis et al. 1998; Flynn et al. 2005). Cerca-Martinez et al. (2000) include these fluvial and lacustrine deposits in the younger part of the Xoconostle conglomerate, which underlies large areas to the south and west of San Miguel Allende. The stratigraphic relations, sedimentary facies, and exposed structures show that the volcanic ash layers accumulated in an actively subsiding graben (Adams 2001). The radiometric ages, paleomagnetic data, and fossils reveal that minor east-west extension had started by 6 Ma.

Thus, the San Miguel Allende basin is contemporaneous with others formed by extension elsewhere in the Basin and Range Province (e.g., Henry and Aranda-Gómez 1992; Ferrari et al. 2002; Aranda-Gómez et al. 2003*b*).

Methods

Stratigraphic sections were measured and carefully described along six arroyos within the San Miguel de Allende graben (fig. 3). The section localities, section names, and ages of the ashes are shown in figure 3 (i.e., Kowallis et al. 1998; Flynn et al. 2005). Samples were collected from volcanic ash beds and from horizons where volcaniclastic input was evident. A high-purity glass fraction was prepared by following the procedures outlined in Perkins et al. (1995) with a few modifications. First, the samples were dried at 550°C overnight to remove moisture, followed by gentle crushing of each ash sample by hand or with a mortar and pestle to separate the glass shards. The samples were then screened through 40-, 80-, and 100-mesh nylon screens. The 40–80 size fraction was passed through a magnetic separator at different current settings to separate magnetic and nonmagnetic minerals from the glass. After magnetic separation, the glass was cleaned ultrasonically for three 2-min intervals in a 5% HF solution to remove surficial contaminants; it was rinsed thoroughly with distilled water between sessions. If calcium carbonate was present, the glass was washed with 10% HCl in an ultrasonic bath for 5 min. Where other purification techniques failed, a small quantity of clean glass shards was picked by hand. Thereafter, the glass was washed with acetone/ethyl alcohol to remove water. Purity of the glass was checked with a petrographic microscope, and the glass shards were mounted in epoxy and polished for microprobe analysis. For seven samples, magnetically separated glass was pulverized and pressed into pellets backed with cellulose for x-ray fluorescence analysis.

Electron probe microanalysis of individual glass shards was performed on a Cameca SX-50. Major elements, Si, Ti, Al, Fe, Mn, Mg, Ca, Na, K, P, F, and Cl were measured on each shard. Typically, 20 shards of glass were analyzed from each ash sample, but only the best analyses were retained. Basaltic glass from the Juan de Fuca ridge and a Hawaiian lava lake, as well as rhyolite from Yellowstone (Jarosewich 2002) were used as standards for calibration (table 1). Microprobe analyses were done with a 4-nanoamp beam current and a 10-μ beam to minimize the loss of Na during analysis of glass. Analytical totals ranged between 93% and 98%, with the amount <100% assumed to be water. For this article, all of the analyses were recalculated to 100%, including analyzed amounts of F and Cl (tables 2, 3). X-ray fluorescence analyses of 19 trace elements were performed with a Siemens SRS-303 using international reference materials (Govindaraju 1994) as standards (tables 2, 3). Major element analyses agreed well the averages of the individual shard analyses by electron microprobe.

Results

The ash beds preserved in the San Miguel de Allende graben were deposited in fluvial overbank environments or in small ponds and lakes (Adams 2001). They are composed mostly of glass shards with minor (<5%) phenocrysts. A visual inspection of the phenocrysts and shards shows them to be angular with little evidence of abrasion, suggesting that the ashes have not, in general, been significantly reworked or mixed with overlying or underlying units. Moreover, the discrete chemical groups indicate that little mixing of ash beds has occurred. The geochemical data for the ash beds have very few outliers (e.g., fig. 4) except for elements such as Na and K that were probably mobile during hydration of the glass. The Miller Place ash (GTO-5a and GTO-11) has two distinct glass populations, but we show below that this is probably a primary feature unrelated to sedimentary mixing. The major element analyses are only on glass shards and so show no contamination by clays, detrital grains, or other nonglassy components. We also went to great efforts to clean the glass for bulk analysis, so the trace element analyses should be little affected by sedimentary admixture.

However, in some cases the single-grain radiometric ages show that some mixing of ash with older material has occurred (Kowallis et al. 1998; Flynn et al. 2005; B. J. Kowallis, unpub. age data). For example, GTO-43 has two populations of zircon fission track ages at 4.4 and 27.6 Ma, while GTO-11 has a scattered zircon fission track age distribution between 4 and 25 Ma. On the other hand, GTO-2c and GTO-12b have only a single population of zircon fission track grain ages. The same patterns can be seen in the single-crystal $^{39}Ar/^{40}Ar$ ages from GTO-5a, where most of the grains average ~3.3 Ma but a few range up to 8.6 Ma. We do not have age data from all of the ash beds but expect that they would be similar to those we have dated. The causes for mixed ages from these samples, which appear to be primary ash-fall beds, may be contamination from older material during deposi-

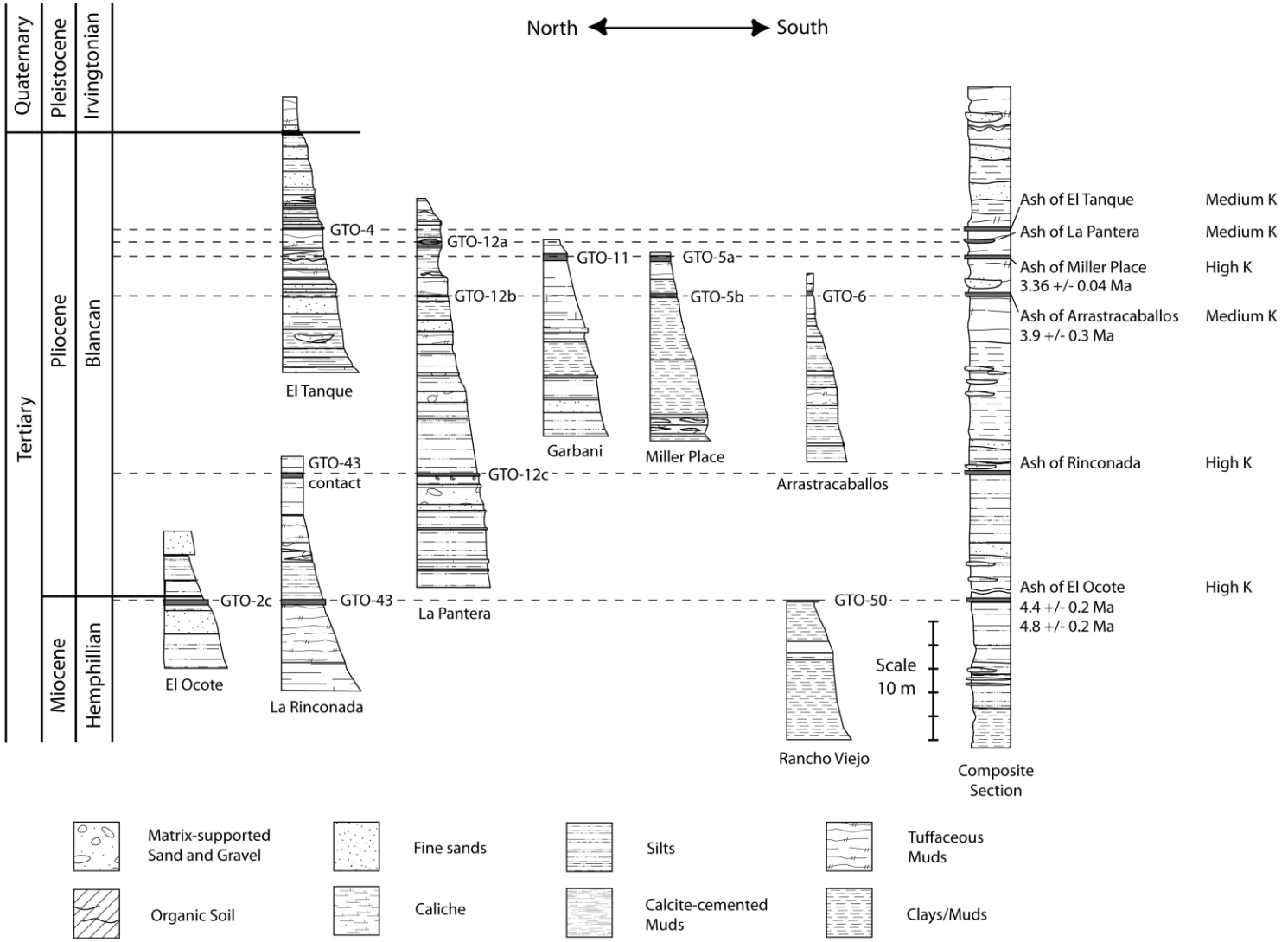

Figure 3. Stratigraphic sections measured in the San Miguel de Allende basin showing the positions of the ash beds, sample locations, and the proposed correlations.

Table 1. Major Element Compositions of Glass Standards Analyzed by Electron Microprobe

Unit	Juan de Fuca	SD (n = 9)	Accepted	Yellowstone	SD (n = 10)	Accepted
SiO_2	50.76	.26	50.81	76.64	.57	76.71
TiO_2	1.81	.04	1.85	.07	.03	.12
Al_2O_3	13.96	.28	14.06	12.29	.20	12.06
Fe_2O_3[a]	11.69	.32	11.84	1.28	.13	1.23
MnO	.20	.05	.22	.04	.04	.03
MgO	6.62	.15	6.71	.03	.01	<.1
CaO	11.08	.18	11.12	.45	.03	.50
Na_2O	2.59	.07	2.62	3.65	.12	3.75
K_2O	.19	.02	.19	4.86	.09	4.89
P_2O_5	.32	.05	.22	.02	.03	<.01
F	.39	.08	…	.20	.06	…
Cl	.02	.02	…	.10	.02	…
Total	99.36	.34	99.64	99.62	.43	99.39

Note. Reported as average of n analyses in weight percent. SD = 1 standard deviation of mean. Accepted values for Juan de Fuca and Yellowstone from Jarosewich (2002).
[a] Fe = Fe_2O_3.

tion, but it is just as likely that contamination occurred during eruption as xenocrysts were incorporated from rock lining the eruptive conduits. Because the phenocrysts are only a small percentage of the total volume of the ash, small amounts of contamination from older deposits show up in the age data but do not significantly affect the glass compositions.

The compositions and ages of the volcanic ash provide insights into the volcanic history of the region during the late Miocene and Pliocene. Electron microprobe analyses were performed on approximately 250 glass shards from 14 samples from the San Miguel de Allende basin. The average compositions of shards from each sample are given in tables 2, 3. (Individual analyses are available at http://geologyindy/byu.edu/faculty/ehc/DataSets.htm.) All of the volcanic glass shards analyzed are rhyolitic, but they range from low- to high-SiO_2 rhyolite. Their silicic compositions are consistent with their typical phenocryst assemblage of quartz, sanidine, and plagioclase accompanied by ubiquitous Fe-Ti oxides, apatite, and zircon (table 1). Mafic silicates vary from bed to bed.

The electron microprobe analyses reveal two distinctive magma series that overlapped somewhat in age. We refer to them as the high-K and medium-K series (fig. 4). In spite of the potential for potassium mobility in hydrated volcanic glasses, both series are distinct in many different compositional parameters, including those for "immobile" elements such as Zr and Ti. The major element compositions form six compositional clusters among the approximately 250 shards analyzed. The six clusters are distinct from each of the others on many chemical variation diagrams (fig. 5). These compositional groups, when combined with stratigraphic position, fossil associations, and paleomagnetic data, allow us to deduce that there were at least six separate eruptions that formed rhyolitic fallout tuffs in the subsiding basin between ~5 and 3 Ma. The high-K series includes the ash beds of El Ocote, Rinconada, and Miller Place, whereas the medium-K series includes La Pantera, Arastracaballos, and El Tanque beds. For some parameters, the highly evolved El Tanque ash bed is transitional to the high-K suite.

Ash of El Tanque (GTO-4). One of the youngest ash beds identified in the basin (fig. 2) is represented by a sample (GTO-4) collected from high (~14 m below the top) in the El Tanque section and is referred to here as the "ash of El Tanque" (fig. 3). It is one of two ash beds deposited in the uppermost Pliocene sediments. It is a laterally continuous, 8-cm-thick, light gray (GSA color chart N8), glassy fallout ash that contains ~5% quartz, sanidine, plagioclase, and biotite. It was thought that this ash would correlate with another ash deposit in the La Pantera section (GTO-12a) only ~1 km away, but the ash of El Tanque is geochemically distinct from any other ash bed in the basin because of its higher SiO_2 and lower Fe_2O_3 content (fig. 5). Flynn et al. (2005) did not show this ash bed in their GTO-4 section, but it probably falls in Chron C2An.2n based upon comparing the position of the ash in our measured section with their section. Thus, this ash bed is probably ~3.1–3.2 Ma following the geomagnetic timescale of Berggren et al. (1995). Vertebrate fossils found at this locality also support this age (Carranza and Miller 1998).

The El Tanque ash is the most silicic member of the medium-K series (fig. 4). Compared with the high-K series at similar silica contents, it has higher Ti, Al, Mg, and Ca. Figure 5 shows its FeO/

Table 2. Major Element Compositions of Glass Shards from Volcanic Ash Beds (El Ocote, La Rinconada, Arastracaballos) Near San Miguel Allende, Mexico

	Ash of El Ocote								Ash of La Rinconada				Ash of Arastracaballos					
	GTO-2c (%, SD)		GTO-50 (%, SD)		GTO-43a (%, SD)		GTO-43k (%, SD)		GTO-43 contact (%, SD)		GTO-12c (%, SD)		GTO-12b (%, SD)		GTO-6 (%, SD)		GTO-5b (%, SD)	
n	20		19		17		18		20		20		10		18		20	
SiO_2	76.91	.26	76.60	.31	76.05	1.06	76.57	.69	73.87	.35	73.84	.38	75.97	.42	75.98	.46	76.24	.47
TiO_2	.07	.03	.09	.02	.09	.04	.07	.03	.20	.03	.20	.02	.24	.04	.25	.03	.22	.06
Al_2O_3	12.55	.23	12.27	.20	12.57	.35	12.52	.51	13.31	.20	13.40	.20	13.48	.22	13.39	.17	13.30	.46
Fe_2O_3[a]	1.16	.12	1.19	.19	1.46	.40	1.33	.30	2.27	.15	2.27	.22	1.48	.18	1.43	.15	1.41	.22
MnO	.02	.03	.06	.08	.04	.05	.04	.05	.14	.09	.12	.06	.05	.06	.07	.08	.05	.05
MgO	.01	.02	.03	.03	.03	.02	.02	.02	.07	.03	.07	.03	.29	.05	.31	.03	.28	.09
CaO	.55	.03	.28	.03	.43	.03	.47	.11	.35	.03	.35	.03	1.54	.07	1.57	.08	1.42	.34
Na_2O	2.58	.43	2.22	.29	2.90	.63	2.51	.28	3.70	.59	4.06	.37	3.55	.14	3.72	.17	3.55	.40
K_2O	5.90	.42	6.93	.28	6.14	.57	6.21	.41	5.91	.72	5.47	.64	3.11	.20	2.97	.26	2.93	.19
P_2O_5	.01	.03	.02	.03	.03	.04	.01	.02	.01	.02	.03	.03	.04	.04	.06	.07	.04	.05
F	.11	.07	.15	.08	.13	.10	.16	.06	.08	.07	.08	.06	.08	.05	.08	.06	.07	.06
Cl	.13	.02	.14	.02	.13	.02	.10	.05	.10	.03	.10	.04	.16	.03	.17	.02	.17	.03
Total	94.58	1.00	96.34	.78	94.27	.79	95.93	.86	95.86	.65	95.61	.63	95.28	1.02	95.52	.88	95.83	.58
Age (Ma)			4.8				4.4		3.9–4.8		3.9–4.8		3.9					
Pmag (Ma)							5.0–5.2						3.3–3.6					
Phenocrysts	qspza		qpsza				qspza		qpsza		qpsza		qpbhxza		qsphxza		qsphxza	
Magmatic series	High K								High K				Medium K					
MALI	Alkali-calcic								Alkalic				Calcic					
FeO/(FeO + MgO)	Ferroan								Ferroan				Magnesian					
T (C°)	875°						880°		920°				847°					
Sr/Y	.3						.4		.2				35					

Note. Composition reported as average of *n* shards in weight percent after normalization to 100%. Phenocryst: q = quartz, s = sanidine, p = plagioclase, b = biotite, h = hornblende, x = pyroxene, z = zircon, a = apatite. MALI = Modified alkali lime index after Frost et al. (2001); *T* (C°) = zircon saturation temperature calculated using Watson and Harrison (1983).
[a] Fe = Fe_2O_3.

(FeO + MgO) ratio is rather low for a high-silica rhyolite. These features combine to make it magnesian and calcic to calc-alkalic in the classification of Frost et al. (2001). Figure 6 shows the normalized trace element pattern has many features typical of subduction-related silicic magmas, including enrichments of large ion lithophile elements (Rb, Ba, and K) compared with high field strength elements like Nb and Ti and a positive Pb anomaly. A large negative P anomaly is the result of apatite fractionation. However, in spite of its high silica contents, the El Tanque ash is not significantly depleted in Sr. Instead, it has a high Sr/Y ratio of ~50 such as those of adakites (Defant and Drummond 1990). A Sr/Y ratio >40 is considered adakitic in dacitic rocks, but the ratio could be lower in rhyolitic magmas where Sr is a compatible element and Y is an incompatible element. Sample GTO-12a has a temperature of 865°C using the Zr concentration in the glass separate (Watson and Harrison 1983).

Ash of La Pantera (GTO-12aA and GTO-12aK). An ash bed high (~5 m below the top of the section) in the La Pantera section is called the "ash of La Pantera." Here it is a lens-shaped deposit that varies in thickness from 80 cm to 1 cm over a distance of only ~10 m and probably filled a depression. This white (GSA color chart N9), glassy ash contains minor amounts of quartz, plagioclase, biotite, hornblende, and pyroxene (<5%). Two samples were collected from this layer within 10 m of one another, and both were analyzed by electron microprobe. Many shards from both samples cluster together in all of the plots (figs. 4, 5), but about half of the shards in one sample (GTO-12aA) are distinctly different from any found in the other sample (GTO-12aK). The anomalous shards are high-silica rhyolites compared with the typical low-silica rhyolite found for the rest of the shards. However, they do not lie on normal magmatic differentiation trends that could connect them to the main population. For example, in shards that have about the same Fe_2O_3 contents, TiO_2 contents are ~0.15 wt% lower in the anomalous shards (fig. 5). Thus, this sample is probably a physical mixture of shards mixed either by reworking of several ash beds or during sam-

Table 3. Major Element Compositions of Glass Shards from Volcanic Ash Beds (Miller Place, La Pantera, El Tanque) Near San Miguel Allende, Mexico

	Ash of Miller Place						Ash of La Pantera						El Tanque	
	GTO-11 (%, SD)		GTO-5a (%, SD)		GTO-5a[a] (%, SD)		GTO-12a A[b] (%, SD)		GTO-12a A[c] (%, SD)		GTO-12a K (%, SD)		GTO-4 (%, SD)	
n	17		11		8		16		6		11		18	
SiO_2	74.57	1.73	70.66	.71	75.14	.16	75.30	2.07	72.97	.74	73.53	.53	77.65	.82
TiO_2	.13	.07	.32	.04	.13	.03	.12	.06	.34	.05	.37	.03	.13	.04
Al_2O_3	12.68	1.25	14.77	.46	12.18	.16	13.06	.71	14.51	.47	14.50	.14	12.83	.23
Fe_2O_3[d]	2.30	.57	3.12	.19	2.43	.18	1.53	.73	2.02	.34	1.97	.15	.67	.16
MnO	.09	.07	.14	.11	.06	.05	.08	.10	.04	.04	.08	.07	.07	.07
MgO	.05	.09	.12	.04	.02	.03	.06	.03	.43	.19	.52	.04	.11	.03
CaO	.34	.26	.64	.08	.22	.02	.44	.10	1.89	.75	2.05	.08	.62	.04
Na_2O	3.83	.79	4.59	.27	3.72	.31	3.08	.84	4.24	.33	3.93	.56	2.52	.60
K_2O	5.64	.81	5.38	.42	5.68	.52	6.10	.59	3.24	1.14	2.72	.16	5.14	1.01
P_2O_5	.04	.05	.04	.05	.03	.05	.01	.02	.06	.03	.07	.05	.02	.04
F	.13	.08	.10	.06	.16	.06	.08	.10	.09	.07	.09	.07	.06	.06
Cl	.20	.04	.12	.03	.23	.02	.13	.02	.18	.04	.16	.03	.16	.04
Total	95.82	.73	96.07	1.02	96.29	1.06	95.31	.77	95.40	1.03	95.86	.72	95.75	1.13
Age (Ma)			3.36						<3.36				<3.36	
Pmag (Ma)			3.3–3.6						3.1–3.2				3.1–3.2	
Phenocrysts	qspbhxza		qspbza						qpbhxza				qspbza	
Magmatic series			High K						Medium K				Medium K	
MALI			Alkalic						Calcic to calc-alkalic				Calc-alkalic	
FeO/(FeO + MgO)			Ferroan						Magnesian				Transitional	
T (C°)			960°						865°				866°	
Sr/Y			.7						17				53	

Note. Composition reported as average of *n* shards in weight percent after normalization to 100%. Phenocryst: q = quartz, s = sanidine, p = plagioclase, b = biotite, h = hornblende, x = pyroxene, z = zircon, a = apatite. MALI = Modified alkali lime index after Frost et al. (2001); *T* (C°) = zircon saturation temperature calculated using Watson and Harrison (1983).

[a] Low-Al_2O_3 shards.

[b] Low-TiO_2 shards.

[c] High-TiO_2 shards.

[d] Fe = Fe_2O_3.

pling of thin ash beds superimposed on one another. In fact, many of the anomalous low-TiO_2 shards in GTO-12aA are indistinguishable from the older ashes of La Rinconada or El Ocote (described below).

The ash of La Pantera is close both stratigraphically and gechronologically to the ash of El Tanque (fig. 3), and it is uncertain which of these two ash beds is older, but paleomagnetic data indicate that this ash bed is in sediments that are younger (uppermost Pliocene) than those of most of the other sections (Flynn et al. 2005). Like the ash of El Tanque, the ash of La Pantera lies in Chron C2An.2n and must be ~3.1–3.2 Ma (Berggren et al. 1995).

The ash of La Pantera belongs to the medium-K series, and like the other members of the series, it is magnesian and calcic to calc-alkalic. Nonetheless, it is distinctive in that it has higher concentrations of TiO_2, MgO, and CaO than any other ash bed in the basin (fig. 5). The La Pantera ash bed shares many of its trace element characteristics with the ash of El Tanque (fig. 6), including low Nb, P, Ti, and Y coupled with a spike for Pb. Its Sr/Y is not as high (~17) as in the El Tanque rhyolite. Zr concentrations imply a temperature of ~865°C, indistinguishable from the El Tanque.

Ash of Miller Place (GTO-5a and GTO-11). Volcanic ash collected from a bed 1 m below the top of the Miller Place section (sample GTO-5a) and from 3 m below the top of the Garbani section (GTO-11) is hereafter referred to as the "ash of Miller Place" (fig. 3). This ash bed is ~2 m below the ash of La Pantera. The ash is a light gray (GSA color chart N8), very fine-grained pyroclastic fall bed that is almost exclusively glass. The GTO-5a sample has only minor quartz, sanidine, plagioclase, and biotite. The GTO-11 sample has these phenocrysts, but it also has traces of amphibole and pyroxene. Ash thickness varies from ~110 cm to <40 cm over a distance of a few meters in one of the measured sections. Both samples come from the same paleomagnetic Chron, C2an.3n (Flynn et al. 2005). A $^{40}Ar/^{39}Ar$ age of 3.36 ± 0.04 Ma (1σ error) on sani-

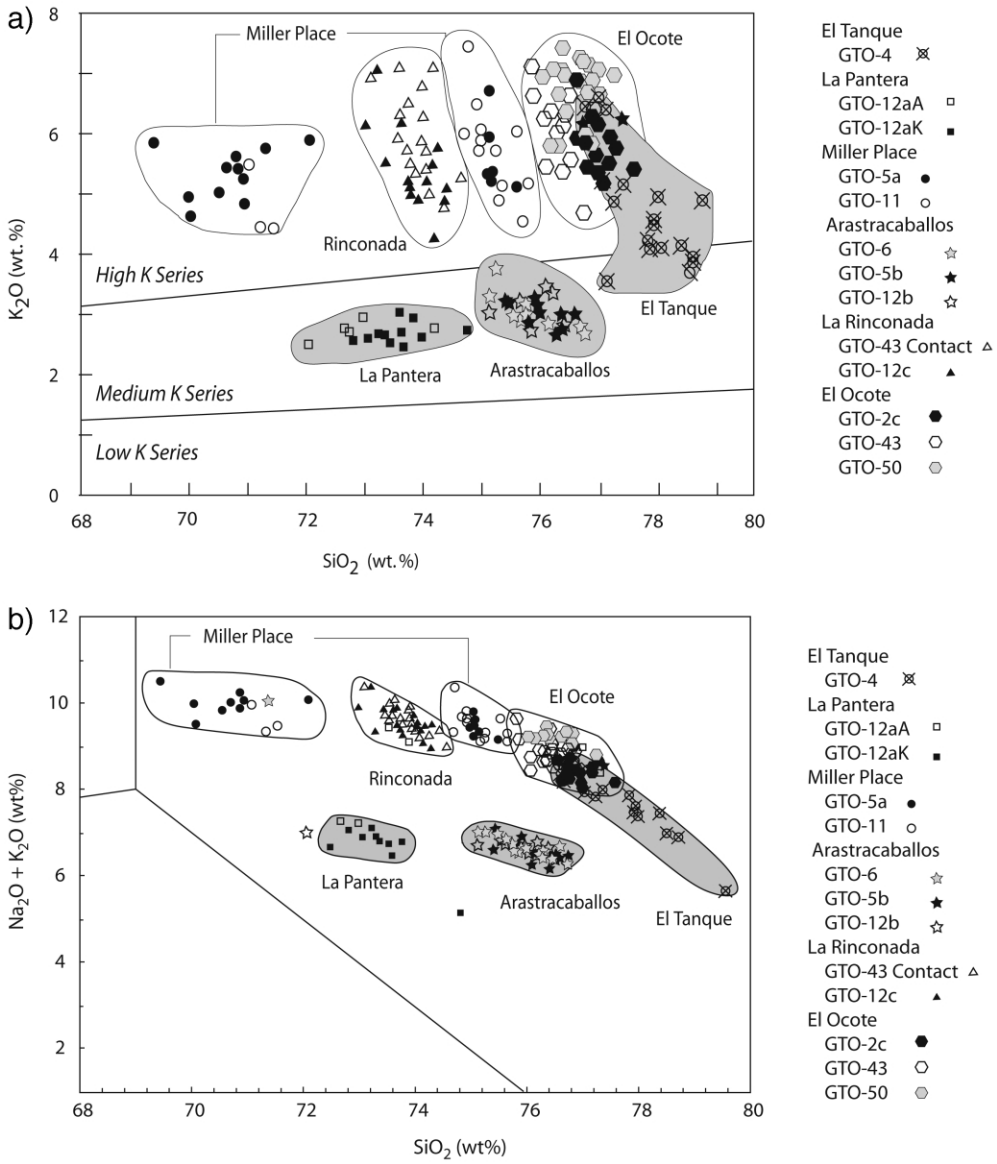

Figure 4. Compositions of glass shards in ash beds from the San Miguel de Allende beds. *a*, K_2O versus SiO_2 chemical variation diagram. Field boundaries are from Ewart (1979). Large variations in K_2O concentrations are probably the result of secondary hydration, but the difference between the medium-K and high-K series is still apparent and is apparent for other less mobile elements (fig. 5). *b*, Total alkali versus silica classification diagram. Electron microprobe analyses of individual glass shards are shown. Groups enclosed with a solid line are our correlations of samples. Medium-K series shown with gray background; high-K series shown with outline.

dine for this ash bed (Kowallis et al. 1998) agrees well with the paleomagnetic age of Chron 2an.3n or 3.33–3.58 Ma (Berggren et al. 1995) and with the ages of the vertebrate fossils (Carranza and Miller 1996).

Both samples of the ash of Miller Place contain two populations of glass, including both low-silica and high-silica rhyolite (figs. 4, 5). The lower SiO_2 shards contain less SiO_2 than any of the other analyzed samples, but both populations of glass shards fall into the high-K magmatic series (fig. 4). The bimodality may have been caused by eruption from a zoned magma chamber or from completely separate eruptions of similar age that were mixed through posteruption depositional processes. We favor the first hypothesis because the phenocrysts and shards are angular with little evidence of abrasion and because we have identified an eruptive

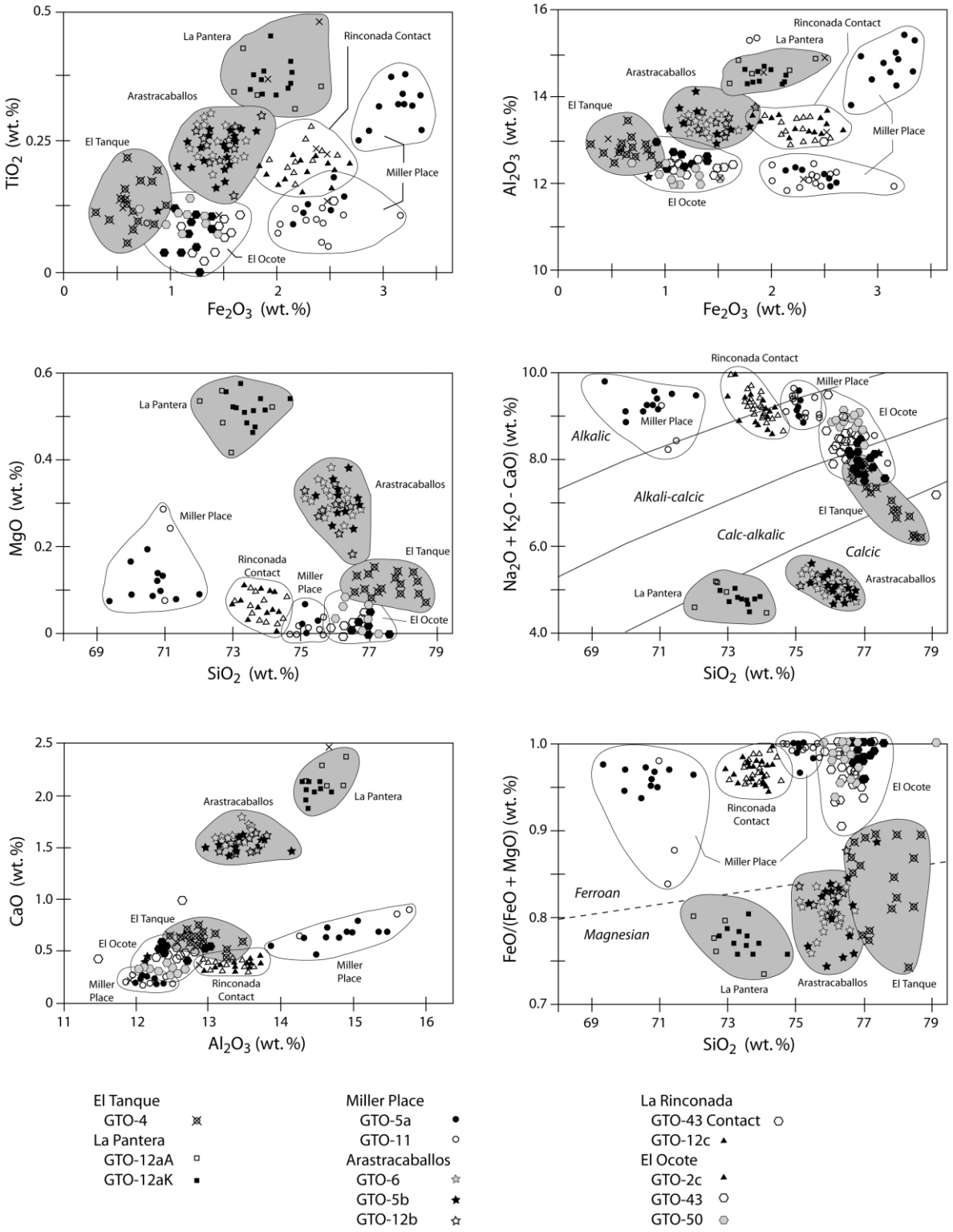

Figure 5. Chemical variation diagrams for the ash beds from the San Miguel de Allende graben. Samples are shown with different symbols and are grouped (*solid lines*) based upon our correlations. Electron microprobe analyses of individual glass shards are shown along with x-ray fluorescence analyses of bulk glass separates (×). Medium-K series shown with gray background; high-K series shown with outline. Fields taken from Frost et al. (2001) and Miyashiro (1974).

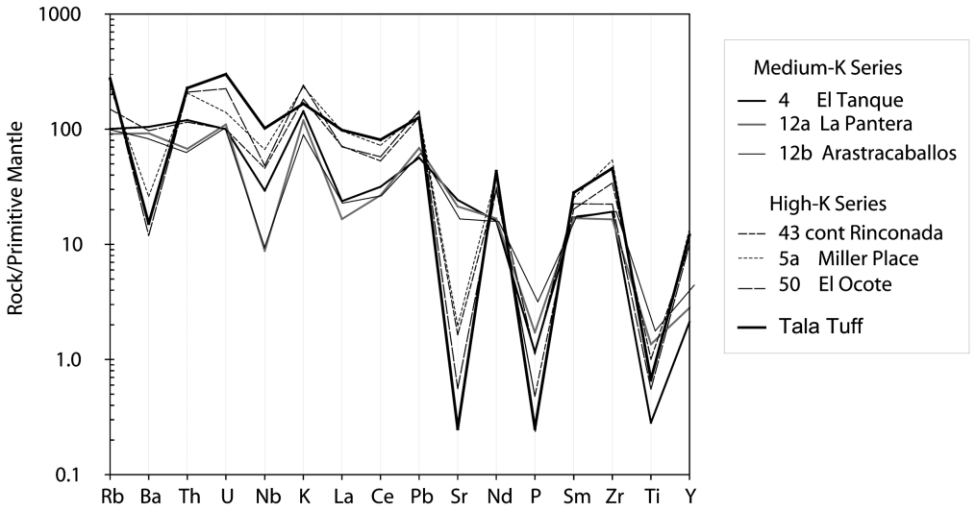

Figure 6. Trace element patterns for rhyolites of the San Miguel de Allende basin. Normalization factors from McDonough and Sun (1995).

source of the same age that also has two types of fiamme—one high-silica and the other low-silica rhyolite. We note that sample GTO-5a has a few single-crystal sanidine ages that range up to 8.6 Ma, but these could be xenocrysts picked up during eruption and may not represent sedimentary reworking.

In the ash of Miller Place, the high-silica shards are comendites (peralkaline rhyolites) with distinctively low Al_2O_3, CaO, and MgO combined with high iron and high Fe/Mg ratios (fig. 5), whereas the lower-silica rhyolites are not quite peralkaline. Nonetheless, both types of rhyolitic glass are alkalic and ferroan in the classification of Frost et al. (2001). The x-ray fluorescence analysis of the Miller Place ash (GTO-5a) plots within or very near the field defined by the high-silica shards, suggesting that these shards comprise the bulk of the ash bed. Biotite and hornblende may be derived from the nonperalkaline portion of the erupted material. As expected from its high-K lineage, the trace element pattern of the ash of Miller Place is very different from the two younger ash beds and similar to other peralkaline rhyolites from the Trans-Mexico Volcanic Belt, such as the much younger Tala Tuff (Mahood 1980). The Miller Place ash has a relatively small negative Nb anomaly, distinctly higher Rb, Th, U, K, Pb, light rare earth elements, and especially Ga, Zn, Y, and Zr (tables 2, 3; fig. 6). The Zr concentrations are high because of the high solubility of zircon in peralkaline melts and typically higher temperatures (~960°C for GTO-5a) of peralkaline rhyolites. This is ~100°C hotter than the medium-K rhyolites. Ba, Sr, P, and Ti are all found in very low abundances as a result of extensive fractionation of feldspars, apatite, and oxides. Like all of the high-K ash beds the Sr/Y ratio is very low (<1; tables 2, 3). The distinctive major and trace element characteristics of the Miller Place ash show that it is an A-type (or within-plate) silicic magma (fig. 7) akin to rift and hotspot related rhyolites the world over.

Ash of Arastracaballos (GTO-6, GTO-5b, and GTO-12b). Volcanic ash from three localities, arroyo Arrastracaballos (sample GTO-6), arroyo Miller Place (sample GTO-5b), and arroyo La Pantera (sample GTO-12b) are all compositionally indistinguishable and are called hereafter the "ash of Arastracaballos." In the Miller Place section, the deposit is ~3.5 m below the ash of Miller Place (fig. 3). Sample GTO-12b is from a laterally continuous, very fine-grained airfall ash ~15 cm thick. It is light gray (N7) to light olive gray (5y 6/1), and it contains ~90% clear glass as well as ~10% phenocrysts of quartz, sanidine, plagioclase, hornblende, and pyroxene as well as the ubiquitous zircon and apatite. Traces of biotite were found only in GTO-12b.

This medium-K ash has higher concentrations of TiO_2, Al_2O_3, MgO, and CaO compared with the high-K ashes of similar silica contents, but it plots between the fields for the other medium-K ashes (El Tanque and La Pantera) in these oxides (figs. 4, 5). Like the other medium-K ashes, it consists of magnesian rhyolite, and because of its low alkali contents, it is calcic (Frost et al. 2001). The trace

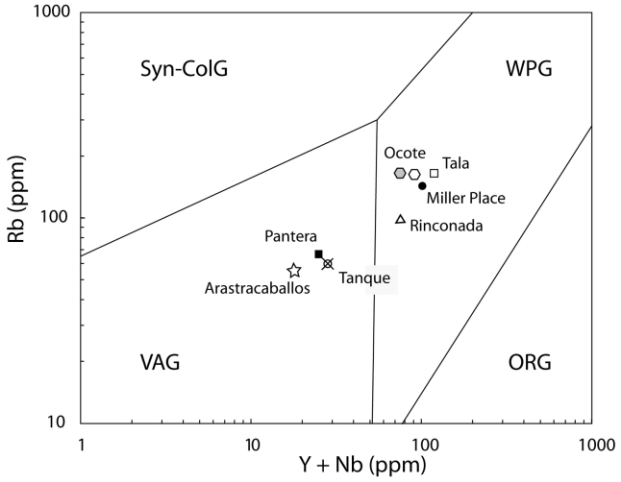

Figure 7. High-K ash beds plot in the within-plate field (WPG) and medium-K ash beds in the volcanic arc field (VAG) on the tectonomagmatic discrimination diagram for silicic igneous rocks of Pearce et al. (1984). Syncollisional granites (Syn-ColG) and ocean ridge granites (ORG) are unlike any of the silicic rocks found in the San Miguel de Allende graben.

element pattern is like the other medium-K ash beds with strong negative Nb and Ti anomalies. It also lacks a deep Sr anomaly and has a Sr/Y ratio of ~35, slightly less than 40, the number used to distinguish adakitic dacites. Zr concentrations imply a temperature of 850°C, similar to but slightly less than the other medium-K ash beds.

Flynn et al. (2005) place GTO-5b and GTO-12b in normal Chron C2An.3n but place GTO-6 in a younger, reversed-polarity Chron C2An.2r. Thus, it is possible that we have sampled two separate deposits that have very similar chemical compositions. However, Chron C2An.3n has an age of 3.33–3.58 Ma (Berggren et al. 1995). A zircon fission track age for GTO-12b is 3.9 ± 0.3 Ma (Kowallis et al. 1998). Although the fission track age overlaps with the geomagnetic polarity age at 2σ, we suggest caution with the interpretation of the paleomagnetic age for this ash bed. Based on the new chemical data, our preferred interpretations are that all three samples come from the same bed and that its eruption age is ~3.9 Ma. Unconformities are common in this continental section, and the interpretation of the paleomagnetic stratigraphy is not straightforward.

Ash of La Rinconada (GTO-43 Contact and GTO-12c). Volcanic ash from high in the La Rinconada section (sample GTO-43 contact) and from a horizon ~30 m below the top of the section in arroyo La Pantera (GTO-12c) correlate geochemically and are hereafter called the "ash of Rinconada." The samples are most distinctive in their Fe_2O_3 and Al_2O_3 concentrations but group together on almost all of the geochemical plots (fig. 5). The GTO-12c sample is from a 25-cm-thick ash bed of essentially aphyric glass and is light gray (N7) to light olive gray (5y 6/1). The purity of this ash diminishes in the upper part of the bed, gradually transitioning into the overlying mudstone. However, the lower contact ash is sharp and easily identified. No magnetic or radiometric dates are available for this ash layer, but its stratigraphic position between dated layers suggests an age between 4.8 and 3.9 Ma. In the La Pantera section, it is ~15 m below the 3.9-Ma ash of Arrastracaballos (fig. 3). Vertebrate fossils are consistent with this assignment (Carranza and Miller 1998).

The ash of Rinconada also erupted from a high-K magmatic system, and like other members of this series, it has characteristically high Fe_2O_3 and Fe/Mg ratios along with low MgO, TiO_2, and Ca/Al ratios (figs. 4, 5). Like all of the other high-K ashes, it is ferroan, and although it is not quite peralkaline like the ash of Miller Place, in terms of its modified alkali lime index, it is alkalic and has high Zr concentrations, suggesting it was hot when erupted (920°C). The trace element pattern of the ash of Rinconada is like the other high-K ashes, except it has much higher Ba, so the pattern between Rb, Ba, Th, and U is almost flat (fig. 6). The high Ba content suggests that it has not experienced as much K-feldspar fractionation as the other high-silica rhyolites.

Ash of El Ocote (GTO-2c, GTO-43, and GTO-50). Glass shards from the oldest ash bed in sections at La Rinconada (sample GTO-43), El Ocote (sample GTO-2c), and near Rancho Viejo (sample GTO-50) are geochemically distinctive (e.g., Fe_2O_3 and TiO_2 in fig. 5). Because of their stratigraphic positions and compositions, they are thought to correlate and are hereafter referred to as the "ash of El Ocote." Small antithetic faults near the GTO-43 locality offset this unit by ~1 m in some areas, demonstrating postdepositional faulting. This ash is light gray (N7), mostly glass, and the most indurated of any ash deposit from the basin. Only traces of quartz, plagioclase, sanidine, as well as zircon and apatite have been identified in mineral separates. Mafic silicates were not found in any of the samples. Its thickness is ~10 cm, and it appears to be fairly laterally continuous.

Vertebrate fossils show that the ash of El Ocote is Hemphillian (Late Miocene) and is the oldest of the ash beds from any of our sections. Two ana-

lytically indistinguishable zircon fission track ages (Kowallis et al. 1998) have been determined for this ash bed: GTO-43, with an age of 4.4 (±0.3) Ma, and GTO-2c, with an age of 4.8 (±0.3) Ma. Flynn et al. (2005) tentatively place the GTO-2c sample locality in Chron C3n.4n with an age of 4.98–5.23 Ma (Berggren et al. 1995), but they place the GTO-43 sample in Chron C3n.3n with an age of 4.80–4.89 Ma. (There is no paleomagnetic data for GTO-50.) Based on their distinctive chemical compositions, we conclude that all three samples come from the same ash bed and are most likely within normal Chron C3n.3n. This is in better agreement with the fission track ages and also with the presence of vertebrate fossils of Hemphillian age.

The El Ocote ash bed is the most silicic of the high-K series ashes yet found in the San Miguel Allende basin. Like the Rinconada ash, it is not peralkaline; it is also ferroan and alkali-calcic because it has slightly lower Na_2O and higher CaO than the other high-K rhyolites. Complementing its high silica concentration are its very low concentrations of MgO, CaO, Fe_2O_3, and TiO_2 (fig. 5). Its higher concentrations of Rb, Y, Nb, Pb, Th, and U and lower Ti, Zr, Sr, and Ba show that it erupted from a cooler (880°C for the zircon saturation temperature) and more evolved magma than the younger ash of Rinconada (920°C). Nonetheless, it is still hotter than any of the medium-K ash beds that have zircon saturation temperatures ranging from 850° to 865°C.

Eruptive Sources for Ash Beds

Based on thickness, continuity, sorting, and the character of the interlayered sedimentary rocks, these ash beds were deposited as pyroclastic fall into fluvial and lacustrine environments (Adams 2001). As such, they may reveal much about the style and geochemistry of volcanism in the broader region. The most likely sources for the ash beds are of course in the nearby east-west-trending arc of late-Miocene-to-Pliocene age that lies just north of the active Trans-Mexican Volcanic Belt (fig. 1). Within the Miocene-Pliocene arc, large silicic caldera-and-dome complexes are more common than in the younger volcanic belt, with its large, andesitic stratocones and other mafic monogenetic volcanoes with associated lava flows (e.g., Nixon et al. 1987; Valdéz -Moreno et al. 1998; Aguirre-Díaz and López-Martínez 2001). Below we speculate on the correlation of the fallout tuffs with their ignimbrite and caldera sources.

The nearest large silicic caldera is the Amazcala caldera (Aguirre-Díaz and López-Martínez 2001), but all known activity is too old to correlate with the ash deposits in the San Miguel de Allende graben. The younger Amealco caldera (Aguirre-Díaz 2004) lies ~100 km southeast of San Miguel de Allende and was active from ~5 to 3 Ma (fig. 1). At 2.9 Ma, the El Rincón rhyolite lava dome complex was emplaced 15 km north of the Amealco caldera (Aguirre-Díaz and McDowell 2000). This slightly peraluminous, high-SiO_2 rhyolite contains 4.9% K_2O and has an SiO_2 content of 76%.Tephra from this rhyolite may be the youngest volcanic deposit in the San Miguel Allende basin, that is, the ash beds of El Tanque or La Pantera, both of which are part of the medium-K series. It is unknown whether the Amealco rhyolites carry the distinctive trace element compositions (e.g., high Sr/Y and low Mg/Fe) of the San Miguel Allende ash beds, making this correlation tenuous at best.

The Guadalajara ignimbrite is 3.3 Ma (Gilbert et al. 1985; Mahood et al. 1985) and contains fiamme with chemical compositions similar to the glass shards of the ash of Miller Place, which has a $^{40}Ar/^{39}Ar$ age of 3.36 Ma (Kowallis et al. 1998). Like the ash of Miller Place, the Guadalajara ignimbrite contains two populations of comenditic fiamme, a high-silica and a low-silica rhyolite. Except for the relatively mobile alkalis, the fiamme have compositions indistinguishable from the shards in the ash of Miller Place. Traces of sanidine are accompanied by pyroxene and amphibole as in the ash of Miller Place, but no biotite is reported in the ignimbrite. Nonetheless, we are confident that the two units correlate because of the age, peralkaline character, and the presence of two populations of distinctive glass.

Five rhyolitic tephras associated with intracaldera lava domes erupted in and near the Amealco caldera between 3.9 and 3.7 Ma (Aguirre-Díaz and McDowell 2000). One of these, the Coronita, is a 3.72 ± 0.27-Ma medium-K rhyolite. This is about the same age as the medium-K ash of Arrastracaballos (3.9 ± 0.3 Ma), but it is unknown whether the Coronita rhyolite has the distinctive character of the medium-K fallout tuffs in the San Miguel de Allende graben.

A possible source for the ash of La Rinconada is the Huichapan Tuff, which erupted 4.2 Ma (Aguirre-Díaz and López-Martínez 2001) from a small caldera of the same name ~200 km southeast of the San Miguel de Allende basin (fig. 1). The age of the Rinconada ash is poorly constrained as being between ~4.8 and 3.9 Ma. The Huichipan Tuff is a widespread, ferroan rhyolitic ignimbrite composed almost exclusively of glass, with only 2%–10% volume quartz and K-feldspar (Aguirre-Díaz and Mc-

Table 4. Trace Element Compositions (ppm) of Glass Separates from Volcanic Ash Beds near San Miguel Allende, Mexico

Unit sample	El Tanque GTO-4	La Pantera GTO-12A	Miller Place GTO-5A	Arastracaballos GTO-12BM	Rinconada GTO-43C	El Ocote GTO-50	El Ocote GTO-43	G-2 analysis	G-2[a] accepted
V	5	61	7	37	3	5	3	35	36
Cr	5	13	5	17	4	6	5	10	9
Ni	<2	<2	<2	<2	<2	<2	<2	2	5
Cu	<2	19	9	15	5	1	4	10	11
Zn	24	50	109	44	93	56	90	82	86
Ga	17	17	24	15	21	16	17	22	23
Rb	60	62	139	55	89	163	163	174	170
Sr	485	350	39	427	10	11	24	494	478
Y	9	20	58	12	45	43	60	12	11
Zr	201	213	568	173	388	235	265	308	309
Nb	19	7	44	6	30	32	33	12	12
Ba	691	566	172	608	641	79	111	1904	1882
La	15	16	63	11	46	46	53	87	89
Ce	53	46	122	45	89	97	134	165	160
Nd	<20	21	50	<20	39	38	51	54	55
Sm	7	8	10	7	8	9	14	8	7
Pb	9	10	21	10	19	22	24	31	30
Th	10	5	17	5	9	17	19	23	25
U	2	<2	3	2	<2	5	3	2	2

[a] G-2 composition from Govindaraju (1994).

Dowell 2000). Milan et al. (1993) report limited major element data for the Huichapan Tuff that are consistent with this interpretation, but there is much variability in the analyses, making the correlation less than certain.

The San Gaspar ignimbrite from near Guadalajara, Mexico, is a crystal-rich dacitic tuff that is ~4.8 Ma (Gilbert et al. 1985). Although its age is appropriate, its composition and mineralogy are unlike the 4.4–4.8-Ma rhyolite ash of El Ocote, the oldest in the San Miguel Allende basin. Near the city of Tepic in far western Mexico (fig. 1), a rhyolite ash flow also erupted 4.6 ± 0.2 Ma (Nixon et al. 1987). This is also close to the age of the ash of El Ocote, but tephra would need to have spread ~450 km east of Tepic to reach San Miguel de Allende. Because it lies <100 km away, a rhyolitic tuff from the Amealco caldera (fig. 1) is a more likely source for the ash of El Ocote. Several major ignimbrites erupted from the caldera ~4.7 Ma (Aguirre-Díaz and McDowell 2000), which is within the time span estimated for El Ocote. The Amealco III ignimbrite, a high-K ash, is the most like El Ocote, but there is insufficient compositional data to establish a correlation with any certainty (Aguirre-Díaz 2001).

Only one of these correlations to possible source regions can be strongly substantiated (the Guadalajara ignimbrite and the ash of Miller Place). However, there are several good possibilities for the sources of several of the other ash beds in the San Miguel Allende basin. The fact that most of these sources are 100–300 km away suggests that these pyroclastic fall deposits may be widespread and that geochemical fingerprinting of these chemically distinctive ash beds may provide a way to correlate from the San Miguel de Allende basin into surrounding basins, where similar fossiliferous sediments are found.

Implications of the Geochemical Data for the Origin of the Silicic Magma Series

The identification of two distinctive magmatic series within the ash-fall deposits of the north-trending San Miguel de Allende graben has important implications for the volcano-tectonic evolution of this part of Mexico. In this section, we first compare the high-K and medium-K series and then consider their tectonic implications. The high-K series includes the ashes of Miller Place, La Rinconada, and El Ocote; the medium-K series consists of the ash beds of Arastracaballos, La Pantera, and El Tanque (tables 2–4). The two oldest ash beds are high-K, and the two youngest are medium-K; there is overlap between the two types of ash between 3.9 and 3.4 Ma. In fact, there may be no temporal trend because both medium-K and high-K volcanism have continued to the present (e.g., volcanism in the main volcanic belt versus the peralkaline Sierra La Primavera center near Guadalajara).

In addition to markedly different K_2O concentrations, the $FeO^*/(FeO^* + MgO)$ ratios exceed 0.9 in the high-K series, and all are ferroan (Frost et al.

2001; or tholeiitic as used by Miyashiro 1974). These high Fe/Mg ratios are probably the result of crystallization at rather low oxygen fugacities. Because of their high alkali contents, the ash beds in the high-K suite are mostly alkalic to alkali-calcic (Frost et al. 2001). Compared with the medium-K series at a given SiO_2 content, the rhyolites of the high-K series have low TiO_2, Al_2O_3, MgO, and CaO, and they have high Fe_2O_3 and total alkalis. Indeed, some members of the high-K series are peralkaline. Many researchers have concluded that ferroan silicic magmas like these are derived from reduced magmas (either tholeiitic or mildly alkalic basalts) by fractional crystallization or by partial melting of basaltic sills and dikes lodged in the crust (e.g., Frost and Frost 1997). This would best explain their low fH_2O (indicated by a general lack of hydrous phenocrysts), low fO_2, high magmatic temperatures (860°–950°C), trace element patterns, and overall alkalic character. Experiments by Nekvasil et al. (2004) show the feasibility of a fractionation path leading from basalts to high-silica rhyolites like these.

In contrast, almost all of the medium-K ashes have $FeO^*/(FeO^* + MgO)$ ratios <0.9 and are magnesian (Frost et al. 2001; or calc-alkaline in the sense of Miyashiro 1974). Using the modified alkali-lime index of Frost et al. (2001), all of the medium-K ashes are calcic to calc-alkalic. The major element compositions of the rhyolites of the medium-K series with their low Fe/Mg ratios are similar to subduction-zone rhyolites that follow relatively oxidized differentiation trends (Ewart 1979) and are apparently similar to other rhyolites in the Mexican Volcanic Belt (Aguirre-Díaz et al. 1998). In addition to their oxidized character, all of the medium-K ash beds have hydrous phases (hornblende and/or biotite) and lower eruption temperatures (≤865°C) than the high-K series.

The trace element patterns (negative Nb and Ti anomalies and enrichments in soluble large ion lithophile elements) of the medium-K rhyolites are also consistent with a subduction origin. In addition, the ash beds of the medium-K series have Sr/Y ratios that range from 17 to 50—some are high enough to be considered adakites as defined by Defant and Drummond (1990) and have Sr/Y >40. Even Sr/Y ratios smaller than this are high for high-silica rhyolites, which typically have strong depletions of Sr (compared with adjacent elements on a normalized trace element diagram; fig. 6). This fact implies that the medium-K rhyolites were derived by differentiation of dacitic magmas that had large positive Sr anomalies. Feineman et al. (2001) propose that the adakite trace element signature is transported to the mantle by Sr-rich fluids from the breakdown of lawsonite to form garnet and zoisite. On the other hand, most petrologists relate the formation of adakites to melting of gabbroic rocks at high pressure (>20 kb) where plagioclase is not stable and garnet is stable. Partial melting then creates Sr-rich and Y-poor liquids because there is no plagioclase to retain Sr in the solids and because abundant garnet retains Y. Gómez-Tuena et al. (2003) and Ferrari (2004) conclude that Miocene adakites are common in a belt north of the present Trans-Mexican Volcanic Belt and that they formed by partial melting of the subducting slab during a significant plate reorganization. We concur and suggest that the slab rollback or breakoff envisioned by Ferrari (2004) created conditions where hot mantle came in contact with basaltic rocks and sediments of the oceanic crust. Although the subduction of hot, young lithosphere is commonly invoked to explain why a slab could melt, Yogodzinski et al. (2001) hypothesize that slab melting may occur where hot mantle flows around the edge of a torn subducting plate.

On the other hand, the ferroan high-K rhyolites are more like those erupted in bimodal suites above hotspots or in continental rifts such as the Miocene and younger A-type rhyolites of the Basin and Range Province (e.g., Christiansen et al. 1986). The trace element patterns are generally consistent with this interpretation as well. For example, the high-K rhyolites fall in the within-plate granite field in the tectonomagmatic discrimination diagrams of Pearce et al. (1984) and in the A-type granite field in the discriminant diagrams of Whalen et al. (1987). In contrast, the medium-K ash beds plot consistently with silicic magmas formed at active continental margins. Modest Nb and Ti depletions and enrichments in Pb (fig. 6) set the high-K series apart from rhyolites erupted on ocean islands and well-developed rifts. These transitional trace element characteristics are also found in the Pleistocene Tala Tuff erupted near Guadalajara (Mahood 1980). Perhaps this trace element signature indicates crustal contamination of mantle-derived magmas or, more likely, considering the peralkaline character of the ash of Miller Place, partial melting of mantle previously metasomatized to some extent by subduction zone fluids.

The ages, regional setting, and chemical compositions combine to suggest that the rhyolites found in the San Miguel de Allende basin were formed by different processes and from different sources that were tapped simultaneously during detachment and subsequent rollback of the subducting Cocos plate (fig. 8). Following detach-

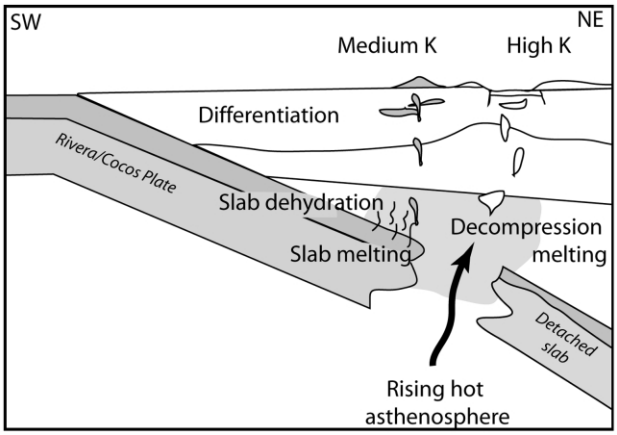

Figure 8. Schematic cross-section showing plate tectonic reconstruction of the Trans-Mexican Volcanic Belt ~5 to 3 Ma. Plate reorganization led to slab breakoff and rollback. Breakoff allowed hot mantle to well through the plate. Melting of the slab produced parental dacitic magmas that differentiated to form the medium-K series with its distinctive adakitic character. Magmas derived by decompression melting of upwelling asthenosphere may have differentiated to form the silicic magmas of the high-K series.

ment, adakitic magmas may have formed by melting of the broken edge of the oceanic lithosphere as hot asthenospheric mantle welled up through the break. Dehydration of the slab and interaction between the slab melts and the mantle wedge further modified the parental magmas. These magmas rose and differentiated to form low-K rhyolites that erupted and accumulated in a simultaneously formed extensional basin. In addition, as the asthenosphere rose through the gap in the slab, decompression melting led to the formation of mafic magma with ocean island basalt affinities. Extensive differentiation of these mafic magmas led to the high-K series.

Two examples of these contrasting processes can also be cited with reference to the mafic magmatism of the region. Miocene to Pleistocene basalts crop out in and around the city of Guadalajara, Mexico (Moore et al. 1994) and are associated with younger predominantly silicic volcanism in the Guadalajara region. The basalts contain two contemporaneous magma types distinguished by contrasting major and trace element compositions, one that is characteristic of a subduction-related magma source and the other of an asthenospheric source (Moore et al. 1994). In addition, Petrone et al. (2003) and Righter and Rosas-Elguera (2001) have contrasted an Na-alkaline series with a contemporaneous calc-alkaline series in mafic lavas of western Mexico. They postulate that magmas of the Na-alkaline series formed by decompression melting of the asthenosphere and simultaneous interaction with fluids being released from the subducting slab (or with the overlying, already metasomatized lithospheric mantle) to take on some trace element characteristics of subduction zone magmas. Differentiation of these magmas, plus or minus crustal contamination, could produce the high-K series described here. All of the ash beds that belong to this series have strong A-type characteristics, and some are distinctly peralkaline.

Conclusions

Our conclusions are based on interpretations of rocks found within a single relatively small extensional basin in central Mexico. Nonetheless, because they include fallout ashes apparently erupted from a large portion of central Mexico and because they lie in the transition between the Sierra Madre Occidental and the Trans-Mexican Volcanic Belt, their relations may help us unravel the geologic evolution of a much larger region. We conclude that Miocene to Pliocene (5–3 Ma) rhyolitic fall-out ash was deposited in fluvial and lacustrine environments during subsidence of the San Miguel de Allende graben of central Mexico. The compositions of glass shards from 14 localities reveal that there were at least six separate eruptions of two contrasting types of rhyolite. Their radiometric dates constrain the timing of small-scale extension and serve as regional markers for stratigraphic correlation among important vertebrate fossil localities (e.g., Miller and Carranza-Castañeda 2001).

The two different rhyolite series sampled by the eruptions are a high-K series and a medium-K series. The medium-K magmatic series includes the ashes of La Pantera, Arastracaballos, and El Tanque that erupted from ~3 to 4 Ma. The high-K series includes the ashes of Rinconada, Miller Place, and El Ocote, which range in age from 3.4 to ~4.8 Ma. The high-K rhyolites are alkali-calcic to alkalic, ferroan, and marginally peralkaline ($Na_2O + K_2O > Al_2O_3$) with high eruption temperatures, low water and oxygen fugacities, high alkalis and Fe_2O_3, and low Al_2O_3, MgO, and CaO compared with the medium-K series, which is mostly magnesian and ranges from calcic to calc-alkalic. The high-K rhyolites have more in common with rift-related magmatic systems than with those in subduction-related calc-alkalic arcs. On the other hand, the medium-K rhyolites are similar to magmas erupted from con-

tinental magmatic arcs and island arcs related to the subduction of young oceanic lithosphere.

In short, the silicic volcanic ash beds accurately reflect the two major types of magmatism occurring in central Mexico, where a subduction-related series of magnesian calc-alkalic magmas erupt to make large central volcanoes, and continental rifting subparallel to the arc (especially along the Tepic-Zacoalco and Chapala grabens) creates caldera-related magmatic systems erupting ferroan, alkalic, and even peralkaline magmas. This twofold division is similar to that identified in the mafic rocks, where alkalic lavas with an ocean island basalt signature (Righter and Rosas-Elguera 2001; the Na-alkaline series of Petrone et al. 2003) are contemporaneous with mafic calc-alkaline basalts and andesites with a subduction-zone character (Luhr et al. 1989). Rifting could be associated with retreat of the subducting Rivera plate (Rosas-Elguera et al. 1996; Ferrari et al. 1999) or slab breakoff (Ferrari 2004).

ACKNOWLEDGMENTS

This research was funded by the National Science Foundation (EAR-9902898) and Brigham Young University. We appreciate the support given by the Instituto de Geología at Universidad Nacional Autónoma de México in Juriquilla, México, and Anadarko Petroleum Corporation. We also thank D. Tingey and M. Dorais for providing laboratory and technical assistance and D. Blatter and G. Aguirre-Díaz for helpful reviews and discussion of volcanism in central Mexico. The manuscript was also strengthened by the perceptive comments of the anonymous reviewers and of the editor, A. T. Anderson.

REFERENCES CITED

Adams, A. 2001. Late Cenozoic sedimentation in the San Miguel de Allende basin, Guanajuato, Mexico. MS thesis, Brigham Young University, Provo, UT.

Aguirre-Díaz, G. J. 2001. Recurrent magma mingling in successive ignimbrites from Amealco caldera, central Mexico. Bull. Volcanol. 63:238–251.

———. 2004. The Amealco and Huichapan calderas and related ignimbrites. *In* Field trip guide for Neogene-Quaternary continental margin volcanism: the Mexican Volcanic Belt. International Association of Volcanology and Chemistry of the Earth's Interior Workshop, Mexico City, 46 p.

Aguirre-Díaz, G. J.; Ferrari, L.; Nelson, S. A.; Carrasco-Núñez, G.; López-Martínez, M.; and Urrutia-Fucugauchi, J. 1998. El cinturón volcánico Mexicano: un proyecto multidisciplinario. Union Geofis. Mex. Geos. 18:131–138.

Aguirre-Díaz, G. J., and López-Martínez, M. 2001. Evolución geológica de la caldera de Huichapan, Hidalgo, en base a nuevas edades ^{39}Ar-^{40}Ar. Geosciencias 21: 320–321.

Aguirre-Díaz, G. J., and McDowell, F. W. 2000. Volcanic evolution of the Amealco caldera, central Mexico. *In* Delgado-Granados, H.; Aguirre-Díaz, G. J.; and Stock, J. M., eds. Cenozoic tectonics and volcanism of Mexico. Boulder, CO. Geol. Soc. Am. Spec. Pap. 334:179–193.

Allan, J. F. 1986. Geology of the Northern Colima and Zacoalco Grabens, southwest Mexico: Late Cenozoic rifting in the Mexican Volcanic Belt. Geol. Soc. Am. Bull. 97:473–485.

Aranda-Gómez, J. J.; Godchaux, M. M.; Aguirre-Díaz, G. J.; Bonnichsen, B.; and Martinez-Reyes, J. 2003*a*. Three superimposed volcanic arcs in the southern Cordillera: from the early Cretaceous to the Miocene, Guanajuato, Mexico. *In* Geologic transects across Cordilleran Mexico: guidebook for field trips of the 99th Annual Meeting of the Cordilleran Section of the Geological Society of America, Mexico. Field trip 6. Universidad Nacional Autónoma de México, Inst. Geol. Publ. Especial 1, p. 123–168.

Aranda-Gómez, J. J.; Henry, C. D.; Luhr, J. F.; and McDowell, F. W. 2003*b*. Cenozoic volcanism and tectonics in NW Mexico: a transect across the Sierra Madre Occidental volcanic field and observations on extension related magmatism in the southern Basin and Range and Gulf of California tectonic provinces. *In* Geologic transects across Cordilleran Mexico: guidebook for field trips of the 99th Annual Meeting of the Cordilleran Section of the Geological Society of America, Mexico. Universidad Nacional Autónoma de México, Inst. Geol. Publ. Especial 1, p. 71–122.

Berggren, W. A.; Kent, D. V.; Swisher, C. C., III; and Aubry, M.-P. 1995. A revised Cenozoic geochronology and chronostratigraphy. SEPM Spec. Publ. 54:129–212.

Carranza, O., and Miller, W. E. 1996. Hemphillian and Blancan age felids from central Mexico. J. Paleontol. 70:509–518.

———. 1998. Paleofaunas de vertabrados de Las Cuencas sedimentarias del Terciario Tardio de la Faja Volcanica Transmexicana. Universidad Autonoma del Estado de Hidago, Avances en Investigacion. Paleontol. Verteb. Publ. Especial 1:85–95.

Carranza-Castañeda, O.; Petersen, M.; and Miller, W. E. 1994. Geology of the northern San Miguel de Allende area. Brigham Young Univ. Geol. Stud. 40:1–9.

Cerca Martinez, L. M.; Aguirre-Díaz, G. J.; and López-Martínez, M. 2000. The geologic evolution of the southern Sierra de Guanajuato, Mexico: a documented example of the transition from the Sierra Madre Oc-

cidental to the Mexican Volcanic Belt. Int. Geol. Rev. 42:131–151.
Christiansen, E. H.; Sheridan, M. F.; and Burt, D. M. 1986. The geology and geochemistry of Cenozoic topaz rhyolites from the western United States. Geol. Soc. Am. Spec. Pap. 205, 82 p.
Christiansen, R. L., and Lipman, P. W. 1972. Cenozoic volcanism and plate-tectonic evolution of the western United States. II. Early and middle Cenozoic. Philos. Trans. R. Soc. Lond. 271:249–284.
Defant, M., and Drummond, M. 1990. Derivation of some modern arc magmas by melting of young subducted lithosphere. Nature 347:662–665.
Ewart, A. 1979. A review of the mineralogy and chemistry of Tertiary-Recent dacitic, latitic, rhyolitic, and related salic volcanic rocks. *In* Barker, F., ed. Trondhjemites, dacites, and related rocks. Amsterdam, Elsevier, p. 13–21.
Feineman, M. D.; Hammersley, L.; Bryce, J. G.; and Carmichael, I. S. E. 2001. Compositional consequences of lawsonite breakdown in regions of warm subduction. Abstr. Prog. Geol. Soc. Am., vol. 33, 302 p.
Ferrari, L. 2004. Slab detachment control on mafic volcanic pulse and mantle heterogeneity in central Mexico. Geology 32:77–80.
Ferrari, L.; Garduño, V. H.; Pasquaré. G.; and Tibaldi, A. 1994. Volcanic and tectonic evolution of central Mexico: Oligocene to present. Geofis. Int. 33:91–105.
Ferrari, L.; López-Martínez, M.; and Rosas-Elguera, J. 2002. Ignimbrite flare-up and deformation in the southern Sierra Madre Occidental, western Mexico: implications for the late subduction history of the Farallon plate. Tectonics 21:17–24
Ferrari, L.; Pasquaré, G.; Venegas-Salgado, S.; and Romero-Rios, F. 1999. Geology of the western Mexican Volcanic Belt and adjacent Sierra Madre Occidental and Jalisco block. *In* Delgado-Granados, H.; Aguirre-Díaz, G.; Stock, J. M., eds. Cenozoic tectonics and volcanism of Mexico. Boulder, CO. Geol. Soc. Am. Spec. Pap. 334:65–83.
Ferrari, L.; Petrone, C. M.; and Francalanci, L. 2001. Generation of oceanic island basalt-type volcanism in the western Trans-Mexican Volcanic Belt by slab rollback, asthenosphere infiltration, and variable flux melting. Geology 29:507–510.
Flynn, J. J.; Kowallis, B. J.; Nuñez, C.; Carranza-Castañeda, O.; Miller, W. E.; Swisher, C. C., III; and Lindsay, E. 2005. Geochronology of Hemphillian-Blancan strata, Guanajuato, Mexico, and implications for timing of the great American biotic interchange. J. Geol. 113:287–307.
Frost, B. R.; Barnes, C. B.; Collins, W. J.; Arculus, R. J.; Ellis, D. J.; and Frost, C. D. 2001. A geochemical classification for granitic rocks. J. Petrol. 42:2033–2048.
Frost, C. D.; and Frost, B. R. 1997. Reduced rapakivi-type granites: the tholeiite connection. Geology 25:647–650.
Gilbert, C. M.; Mahood, G. A.; and Carmichael, I. S. E. 1985. Volcanic stratigraphy of the Guadalajara area, Mexico. Geofis. Int. 24:169–191.
Gómez-Tuena, A.; LaGatta, A.; Langmuir, C.; Goldstein, S.; Ortega-Gutiérrez, F.; and Carrasco-Núñez, G. 2003. Temporal control of subduction magmatism in the eastern Trans-Mexican Volcanic Belt: mantle sources, slab contributions and crustal contamination. Geochem. Geophys. Geosyst., vol. 4, doi:10.1029/2003GC000524.
Govindaraju, K. 1994. Compilation of working values and description for 383 geostandards. Geostand. Newslett. 18:1–158.
Henry, C. D., and Aranda-Gómez, J. J. 1992. The real southern basin and range: mid- to late Cenozoic extension in Mexico. Geology 20:701–704.
Henry, C. D.; Price, J. G.; and James, E. W. 1991. Mid-Cenozoic stress evolution and magmatism in the southern Cordillera, Texas and Mexico: transition from continental arc to intraplate extension. J. Geophys. Res. 96:13,545–13,560.
Jarosewich, E. 2002. Smithsonian microbeam standards. J. Res. Nat. Inst. Stand. Tech. 107:681–685.
Kowallis, B. J.; Heaton, J. S.; and Bringhurst, K. 1986. Fission-track dating of volcanically derived sedimentary rocks. Geology 14:19–22.
Kowallis, B. J.; Swisher, C. C., III; Carranza-Castañeda, O.; Miller, W. E.; and Tingey, D. G. 1998. Fission-track and single-crystal $^{40}Ar/^{39}Ar$ laser-fusion ages from volcanic ash layers in fossil-bearing Pliocene sediments in central Mexico. Rev. Mex. Cienc. Geol. 15:157–160.
Lipman, P. W.; Prostka, H. J.; and Christiansen, R. L. 1972. Cenozoic volcanism and plate-tectonic evolution of the western United States. I. Early and middle Cenozoic. Philos. Trans. R. Soc. Lond. 271:217–248.
Luhr, J. F.; Allan, J. F.; Carmichael, I. S. E.; Nelson, S. A.; and Hasenaka, T. 1989. Primitive calc-alkaline and alkaline rock types from western Mexican Volcanic Belt. J. Geophys. Res. 94:4515–4530.
Mahood, G. 1980. Geological evolution of a Pleistocene rhyolitic center: Sierra La Primavera, Mexico. J. Volcanol. Geotherm. Res. 8:199–230.
Mahood, G.; Gilbert, C. M.; and Carmichael, I. S. E. 1985. Peralkaline and metaluminous mixed-liquid ignimbrites of the Guadalajara region, Mexico. J. Volcanol. Geotherm. Res. 25:259–271.
McDonough, W. F., and Sun, S. S. 1995. The composition of the earth. Chem. Geol. 120:223–254.
Milan, M.; Yanez, C.; Navarro-L. I.; Verma, S. P.; and Carrasco-Núñez G. 1993. Geology and major-element geochemistry of the caldera de Huichapan, Hidalgo, Mexico. Geofis. Int. 32:261–276.
Miller, W. E., and Carranza-Castañeda, O. 2001. Late Cenozoic mammals from the basins of Central Mexico. Boll. Soc. Paleontol. Ital. 40:235–242.
Miyashiro, A. 1974. Volcanic rock series in island arcs and active continental margins. Am. J. Sci. 274:321–355.
Moore, G.; Marone, C.; Carmichael, I. S. E.; and Renne, P. 1994. Basaltic volcanism and extension near the intersection of the Sierra Madre volcanic province and the Mexican Volcanic Belt. Geol. Soc. Am. Bull. 106:383–394.

Mooser, F. 1972. The Mexican Volcanic Belt: structure and tectonics. Geofis. Int. 12:55–70.

Nekvasil, H.; Dondolini, A.; Horn, J.; Filiberto, J.; Long, H.; and Lindsley, D. H. 2004. The origin and evolution of silica-saturated alkalic suites: an experimental study. J. Petrol. 45:693–721.

Nieto-Samaniego, A. F.; Ferrari, L.; Alaniz-Alvarez, S.; Labarthe-Hernandez, G.; and Rosas-Elguera, J. 1999. Variation of Cenozoic extension and volcanism across the southern Sierra Madre Occidental volcanic province, Mexico. Geol. Soc. Am. Bull. 111:347–363.

Nixon, G. T.; Demant, A.; Armstrong, R. L.; and Harakal, J. E. 1987. K-Ar and geologic data bearing on the age of the Trans-Mexican Volcanic Belt. Geofis. Int. 26: 109–158.

Noble, D. C. 1972. Some observations on the Cenozoic volcano-tectonic evolution of the Great Basin, western United States. Earth Planet. Sci. Lett. 17:142–150.

Pasquaré, G.; Ferrari, L.; Garduño, V. H.; Tibaldi, A.; and Vezzoli. L. 1991. Geology of the central sector of Mexican Volcanic Belt, states of Guanajuato and Michoacan. Geol. Soc. Am. Map and Chart series MCH 072, 22 p.

Pearce, J. A.; Harris, N. B. W.; and Tindle, A. G. 1984. Trace element discrimination diagrams for the tectonic interpretation of granitic rocks. J. Petrol. 25:956–983.

Perez-Vanzor, J. A.; Aranda-Gómez, J. J.; McDowell, F. W.; and Solorio-Mungio, J. G. 1996. Geologiaz del Volcan Palo Huerfano, Mexico. Rev. Mex. Cienc. Geol. 13:174–183.

Perkins, M. E.; Nash, W. P.; Brown, F. H.; and Fleck, R. J. 1995. Fallout tuffs of Trapper Creek, Idaho: a record of Miocene explosive volcanism in the Snake River Plain volcanic province. Geol. Soc. Am. Bull. 107: 1484–1506.

Petrone, C. M.; Francalanci, L; Carlson, R. W.; Ferrari, L.; and Conticelli, S. 2003. Unusual coexistence of subduction-related and intraplate-type magmatism: Sr, Nd and Pb isotope and trace element data from the magmatism of the San Pedro–Ceboruco graben (Nayarit, Mexico). Chem. Geol. 193:1–24.

Righter, K., and Rosas-Elguera, J. 2001. Alkaline lavas in the volcanic front of the western Mexican Volcanic Belt: geology and petrology of the Ayutla and Tapalpa volcanic fields. J. Petrol. 42:2333–2361.

Rosas-Elguera, J.; Ferrari, L.; Urrutia-Fucugauchi, J.; and Garduño, V. H. 1996. The continental boundaries of the Jalisco block and their influence in the Neogene kinematics of western Mexico. Geology 24:921–924.

Snyder, W. S.; Dickinson, W. R.; and Silberman, M. L. 1976. Tectonic implications for space-time patterns of Cenozoic magmatism in the western United States. Earth Planet. Sci. Lett. 32:91–106.

Stewart, J. A. 1978. Basin-range structure in western North America: a review. *In* Smith, R. B., and Eaton, G. P., eds. Cenozoic tectonics and regional geophysics of the western Cordillera. Geol. Soc. Am. Mem. 152: 1–13.

Valdéz-Moreno, G.; Aguirre-Díaz, G. J. D.; and López-Martínez, M. 1998. El Volcán La Joya, estados de Quéretaro y Guanajuato: un estratovolcán Miocénico del Cinturón volcánico Mexicano. Rev. Mex. Cienc. Geol. 15:181–197.

Watson, E. B., and Harrison, T. M. 1983. Zircon saturation revisited: temperature and composición effects on a variety of crustal magma types. Earth Planet. Sci. Lett. 64:295–304.

Whalen, J. B.; Currie, K. L.; and Chappell, B. W. 1987. A-type granites: geochemical characteristics, discrimination and petrogenesis. Contrib. Mineral. Petrol. 95: 407–419.

Yogodzinski, G. M.; Lees, J. M.; Churikova, T. G.; Dorendorf, F.; Woerner, G.; and Volynets, O. N. 2001. Geochemical evidence for the melting of subducting oceanic lithosphere at plate edges. Nature 409:500–504.

Zúñiga, F. R.; Pacheco, J. F.; Guzmán-Speziale, M.; Aguírre-Diaz, G. J.; Espindola, V. H.; and Nava, E. 2003. The Sanfandila earthquake sequence of 1998, Queretaro, Mexico: activation of an undocumented fault in the northern edge of central Trans-Mexican Volcanic Belt. Tectonophysics 361:229–238.